A COMPARATIVE POD/DMD ANALYSIS OF CANONICAL AND ACTUATED TURBULENT CHANNEL FLOWS

JESÚS GARICANO-MENA[1,*]**, ESTEBAN FERRER**[1]**, NUNO VINHA**[1] **AND EUSEBIO VALERO**[1]

[1] E.T.S. Ingeniería Aeronáutica y del Espacio, Universidad Politécnica de Madrid
Plaza del Cardenal Cisneros, 3, Madrid, 28040, España
* Corresponding author: J. Garicano-Mena, jesus.garicano.mena@upm.es

Key words: turbulent channel flow, flow control, proper orthogonal decomposition, dynamic mode decomposition.

Abstract. Turbulent flow fields contain a wide range of spatio-temporal scales. Direct Numerical Simulation techniques provide an accurate description of turbulent flow fields. This accuracy comes at the expense of high computational cost and memory footprint. In this context, feature detection algorithms are useful tools that help to identify relevant flow structures, their interactions and ulterior evolution. In this contribution, we employ feature detection algorithms to analyze canonical and controlled turbulent channel flows. Specifically, we will apply both Proper Orthogonal Decomposition and Dynamic Mode Decomposition to DNS-generated turbulent channel flow data-bases. The ultimate goal is to reveal whether flow features linked to drag reduction exist and, if that is the case, learn how those structures could be enhanced, thus leading to more efficient drag reduction strategies.

1 INTRODUCTION

Turbulent flow fields contain a wide range of spatio-temporal scales, see 11. Direct Numerical Simulation (DNS) techniques provide a complete description of turbulent flow fields, at least for flows at low to moderate Reynolds number.

Such DNS descriptions are indeed accurate, but this accuracy comes at the expense of high computational cost and memory footprint. In this context, feature detection algorithms are useful tools that help to identify relevant flow structures, their interactions and ulterior evolution.

In this contribution, we employ feature detection algorithms to analyze canonical and controlled turbulent channel flows. Specifically, we will apply both Proper Orthogonal Decomposition (POD, 2) and Dynamic Mode Decomposition (DMD, 16) to turbulent data-bases generated by the DNS solver described in 9.

The actuation considered is the imposition of a spanwise wall velocity that varies sinusoidally with the streamwise coordinate, $w_{wall} \propto \sin(2\pi x / \lambda_x)$, which is known to lead to drag reduction 17.

Snapshot-based variants of the POD/DMD algorithms have been considered, see section 2 for a complete description of the algorithm.

In order to obtain a richer information, both `POD` and `DMD`analyses considering snapshots formed by different flow quantities have been considered: departing from the velocity field (see the pioneering work of 3), we will consider additionally snapshots formed by alternative magnitudes, *e.g.* Reynolds stresses. Moreover, and encouraged by the promising results in the study of laminar-to-turbulent transition in 15, we intend to apply the composite `DMD`method of Sayadi and Schmid 14. This technique considers snapshots assembled by related quantities -e.g flow velocity and skin friction- to uncover relations between both magnitudes.

The ultimate goal is to reveal whether flow features linked to drag reduction exist and, if that is the case, learn how those structures could be enhanced, thus leading to more efficient drag reduction strategies.

2 METHOD

2.1 Feature detection algorithms: `POD` and `DMD`

Dynamic Mode Decomposition (`DMD`) techniques 16, 4, 10 have increased in popularity over the past years and have been applied to a variety of flows, using data from numerical simulations and experiments (e.g. 1, 10, 12, 5).
First, a brief summary of the *snapshot-based* DMD technique, as proposed in 16, is presented. Given a sequence of instantaneous flow fields numbered from 1 to N (*e.g.* taking one or all recorded variables), the following *data matrix* can be constructed:

$$\mathbf{V}_1{}^N = \{\mathbf{v}(t_1), \mathbf{v}(t_2), .., \mathbf{v}(t_N)\}, \tag{1}$$

where the subindex and superindex identify, respectively, the first and last time instants of the sequence. The data is ordered in time, and separated by a constant sampling time interval Δt^s such that: $t_{j+1} = t_j + \Delta t^s$ for all $j = 1, .., N-1$. In the case of linear stability analysis and within the exponential growth region, it is possible to define a linear operator $\mathbf{A}$ (*i.e.* a numerical approximation of the linearised Navier–Stokes operator) such that $\mathbf{v}(t_{j+1}) = \mathbf{A}\,\mathbf{v}(t_j)$. Eq. (1) can then be rewritten as a Krylov sequence (13):

$$\mathbf{V}_1^N = \{\mathbf{v}(t_1), \mathbf{A}\mathbf{v}(t_1), .., \mathbf{A}^{N-1}\mathbf{v}(t_1)\}. \tag{2}$$

For an ordered sequence, Eq. (2) can be equated to Eq. (1):

$$\mathbf{A}\{\mathbf{v}(t_1), \mathbf{v}(t_2), .., \mathbf{v}(t_{N-1})\} = \{\mathbf{v}(t_2), \mathbf{v}(t_3), .., \mathbf{v}(t_N)\}, \tag{3}$$

which can alternatively be written in matrix form as:

$$\mathbf{A}\mathbf{V}_1{}^{N-1} = \mathbf{V}_2{}^N. \tag{4}$$

Next, the Singular Value Decomposition (`SVD`) of the matrix $\mathbf{V}_1{}^{N-1} = \mathbf{U}\mathbf{\Sigma}\mathbf{W}^H$ is obtained, where the superscript H denotes conjugate transposition. The left singular vectors – the columns of $\mathbf{U}$ – correspond to the `POD`modes of the input data sequence. Thus, the snapshot-based `DMD` algorithm requires the calculation of the `POD` modes.

The `SVD` of the snapshot matrix is then inserted into Eq. (4), which yields $\mathbf{A}\mathbf{U}\mathbf{\Sigma}\mathbf{W}^H = \mathbf{V}_2{}^N$. The reduced matrix $\widetilde{\mathbf{S}} = \mathbf{U}^H\mathbf{A}\mathbf{U}$ associated with the initial system described by $\mathbf{A}$, can be rewritten using the former equality as:

$$\widetilde{\mathbf{S}} = \mathbf{U}^H\mathbf{A}\mathbf{U} = \mathbf{U}^H\mathbf{V}_2{}^N\mathbf{W}\mathbf{\Sigma}^{-1}. \tag{5}$$

The reduced matrix $\widetilde{\mathbf{S}}$ is the projection of the matrix $\mathbf{A}$ onto the POD space contained in $\mathbf{U}$, and previously obtained through the `SVD` operation 16.

Once the reduced matrix $\widetilde{\mathbf{S}}$ has been calculated, the reduced DMD modes $\mathbf{y}_i$ can be obtained, as well as the associated eigenvalues μ_i (*i.e.* growth rates $\Re(\mu_i)$ and frequencies $\Im(\mu_i)$ mapped to the unit circle) of the reduced system by solving the eigenvalue problem $\widetilde{\mathbf{S}}\mathbf{y}_i = \mu\mathbf{y}_i$. The approximated eigenmodes of the matrix $\mathbf{A}$ can then be recovered via a projection onto the original space, using relation $\boldsymbol{\phi}_i = \mathbf{U}\mathbf{y}_i$. Eventually, the growth rates and frequencies in the complex half-plane can be recovered from the eigenvalues as: $\lambda_i = \log(\mu_i)/\Delta t^s$.

Finally, note that the `DMD` decomposition allows to expand the data sequence as:

$$\mathbf{v}(t) = \sum_{i=1}^{N} \alpha_i \, \boldsymbol{\phi}_i e^{i\,\lambda_i\,t}. \tag{6}$$

In this contribution, the amplitudes α_i are computed following the formulation in 8. Note that, since only composite `DMD` analyses (based on C_f and either $u'v'$ or λ_2) are considered in this work, we plot the amplitudes weighted by its contribution to the C_f temporal sequence 6.

2.2 Databases description

Feature detection algorithms describe in previous section have been applied to two turbulent channel flows databases generated by the `DNS` solver described in 9. The solver provides *snapshots* of the flow field including the complete velocity field and the λ_2 invariant 11.

In both cases, the channel walls are planar and the simulations have been conducted under the assumption of constant mass flux. The difference in the databases is the boundary condition enforced at the channel walls: in the *reference* case, the classical no-slip boundary condition has been enforced, whereas in the *actuated* configuration, a streamwise variation of the spanwise velocity component w_{wall} is assumed, namely $w_{wall} = W_0 \sin(2\pi^x/\lambda_x)$. Table 1 summarizes the characteristics of both databases. Note how the actuation strategy is effective in proving drag reduction, as $Re_\tau \approx 200$ for the standard channel whereas $Re_\tau \approx 145$ is effectively observed for the actuated channel flow.

Table 1: Turbulent channel flow databases. Summary.

	L_x/h	L_y/h	L_z/h	n_x	n_y	n_z	u_c	u_τ	Re_τ	W_0	λ_x/L_x	N	Memory $[GB]$
Reference							0.7733	0.04198	199.809	$-$	$-$		
	2π	2	π	192	129	192						1025	190
Actuated							0.7824	0.03077	146.488	0.5	1/2		

3 RESULTS

Figures 2 and 3 summarize the results obtained for the reference channel flow when conducting a `POD`/`DMD` analysis on a sequence of composite $u'v'$-C_f snapshots. Fig. 2a shows the singular values retrieved from the `POD` analysis, whereas Fig. 2c presents the dynamic spectrum. As made evident by Fig. 2c, only a reduced number of modes have amplitudes that are relatively important when compared with the largest one. These results are consistent with those reported by Ghebali *et al.* in 6.

Figure 3 shows both the three first `POD` modes (Figs. 3a, 3c, 3e) and the three dynamic modes with largest associated amplitudes (Figs. 3b, 3d, 3f) for the reference configuration. The first `POD` mode, Fig. 3a, presents a spatial structure elongated an aligned with the streamwise direction. The same is true for the dynamic mode with largest amplitude, Fig. 3b. As the singular value index increases, the corresponding `POD` modes show a spatial structure richer in progressively smaller features, *cf.* Figs. 3c and 3e. Dynamic modes associated with progressively lower amplitudes behave similarly, see Figs. 3d and 3f.

Figure 2 also contains the singular value distribution (Fig. 2b) and the dynamic spectrum (Fig. 2c) corresponding to the actuated channel flow. When compared to the reference configuration, in both cases the singular values and the amplitudes are seen to be smaller. This is a reflection of the reduced turbulence activity in the actuated case.

The corresponding modes associated to the actuated channel flow are presented in Figure 4. Note that here the most amplified dynamic mode is steady and relatively similar in shape to that appearing in the reference case. Moreover, note how this mode weighted by the corresponding amplitude α_1 accounts for the major part of the Reynolds stresses, see Fig. 1. Once again, this is in agreement with the results in 6. However, the next mode in importance by amplification shows a radically different aspect, see Fig. 4d: a low $u'v'$ meandering structure, symmetric with respect to the $x^+ \approx 300$ plane is visible. The next relevant dynamic mode, in Fig. 4f, presents again an elongated structure aligned with the streamwise direction: this is reasonable as this mode has a very small λ_i.

A composite DMD analysis based on λ_2-C_f snapshots has also been conducted. The relationships between singular value distributions and dynamic spectra for both the reference and actuated configurations are similar to those shown in Figure 2, and are thus not shown here.

Figure 5 reports the three dynamic modes with largest amplitudes for both the reference and actuated cases. In this case, the spatial distribution of dynamic modes with largest amplitude present already evident differences: the dynamic mode structure is much more *organized* in the actuated case, *cf.* Figs. 5a and 5b. This difference is maintained for the other dynamic modes shown, and it is particularly remarkable for the third mode, compare Figs. 5e and 5f.

4 CONCLUSIONS

In this contribution we have conducted composite `POD`/`DMD` analyses of turbulent channel flow databases obtained with a `DNS` solver. The composite snapshots have been formed by combining
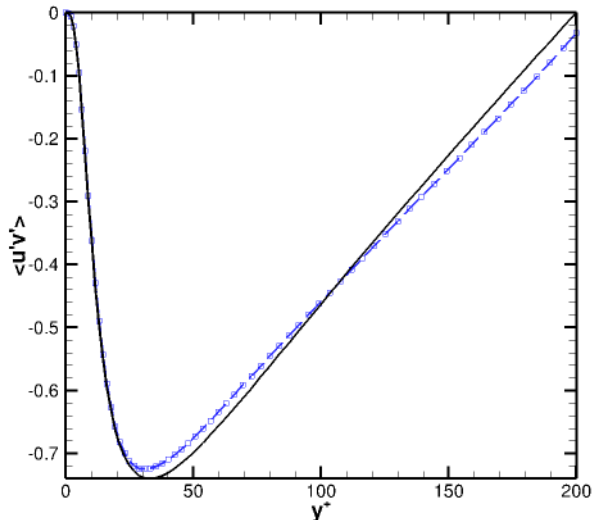
Figure 1: Results for composite analysis on $u'v'$-C_f snapshots for reference channel configuration: $\langle u'v' \rangle_{x,z,t}$ (——) vs contribution from most relevant dynamic mode (—·—·—).

either $u'v'$ or λ_2 spatial fields and C_f.

The beneficial effect of the actuation strategy is observed as a reduction of both the levels of the singular values distribution and the amplitudes corresponding to the most relevant dynamic modes. Regarding the spatial organization of POD/DMDmodes, structures corresponding to the actuated case are more *organized*, as one would expect. The difference in organization is observed particularly well when the analyses are conducted on snapshots built including the λ_2 invariant.

The major problem found so far is related to the management of the large databases employed: storing, accessing and processing the input and transferring and organizing the results obtained are challenging activities. This problem is foreseen to increase as databases at larger Re_τ numbers are considered. A possible avenue to handle this strategy is the application of non-uniform and data compressing formulations of the DMD algorithm, see 7.
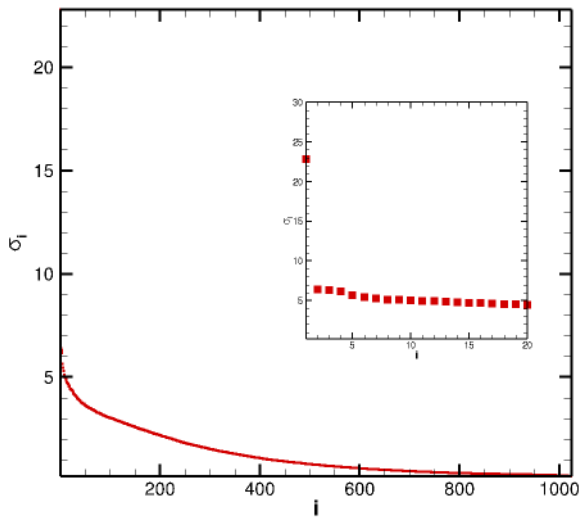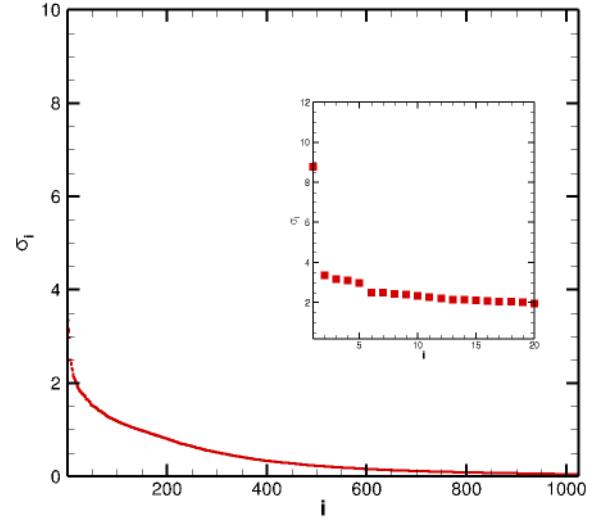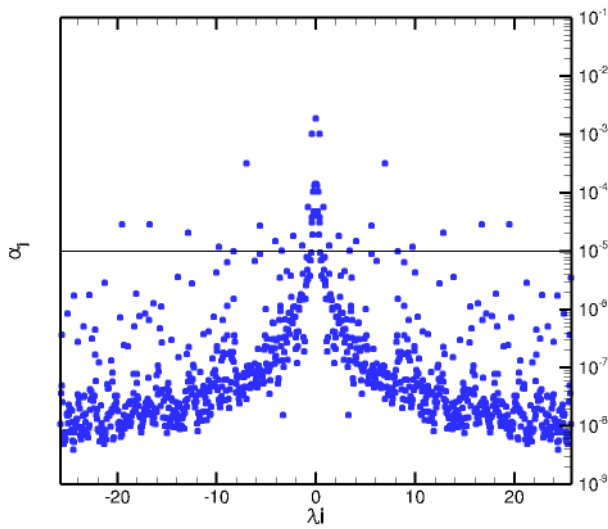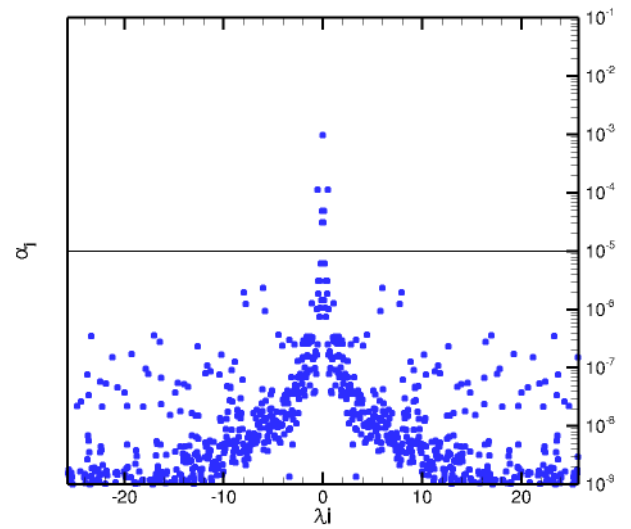
Figure 2: Results for composite analysis on $u'v'$-C_f snapshots for reference (2a and 2c) and actuated channel (2b and 2d)flows: singular values in 2a and 2b; amplitudes of dynamic modes in 2c) and 2d.
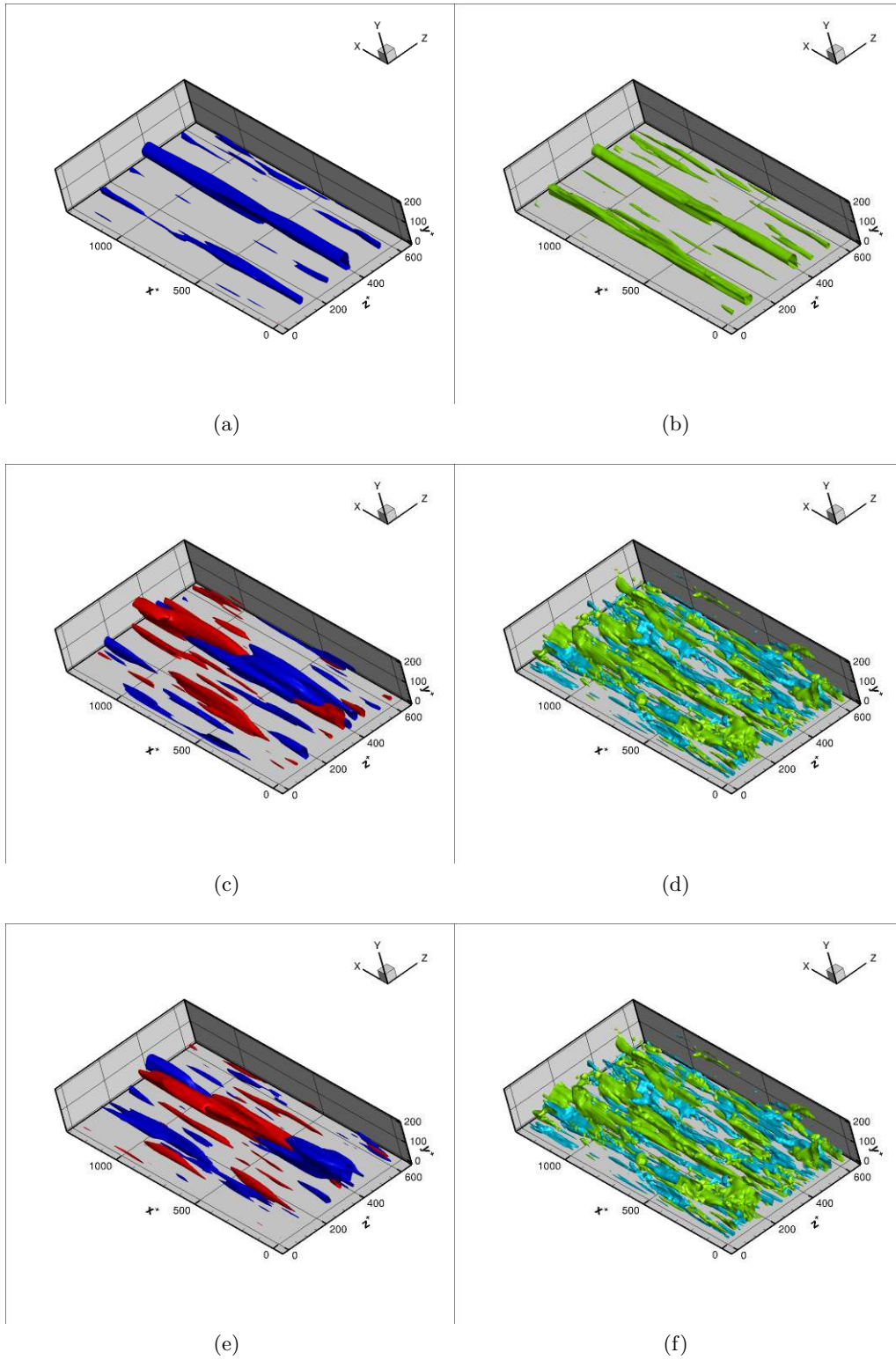
Figure 3: Results for composite analysis on $u'v'$-C_f snapshots for reference channel flow: first POD modes in (a), (c), (e); most relevant dynamic modes in (b), (d), (f).
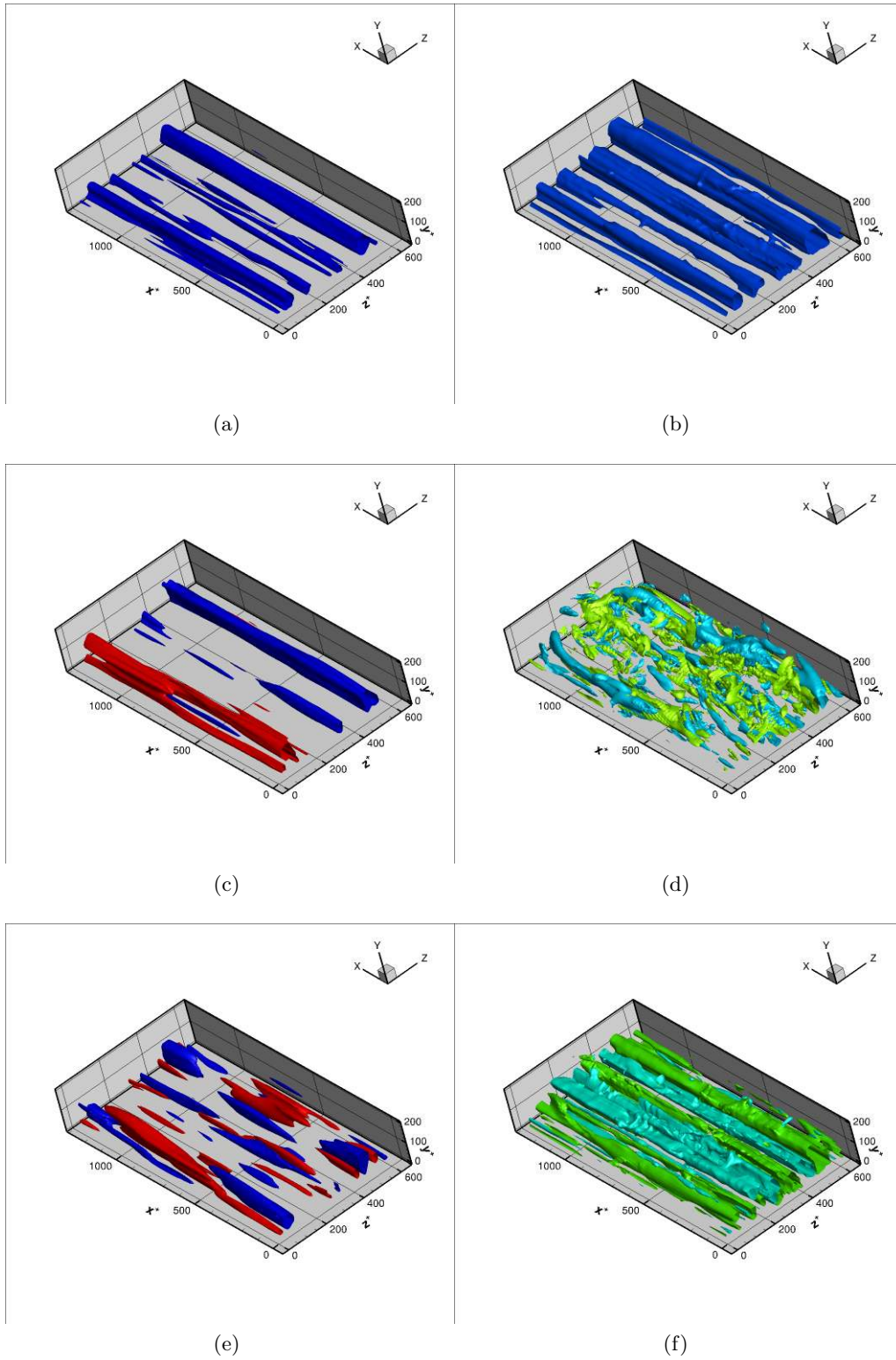
Figure 4: Results for composite analysis on $u'v'$-C_f snapshots for actuated channel flow: first POD modes in (a), (c), (e); most relevant dynamic modes in (b), (d), (f).
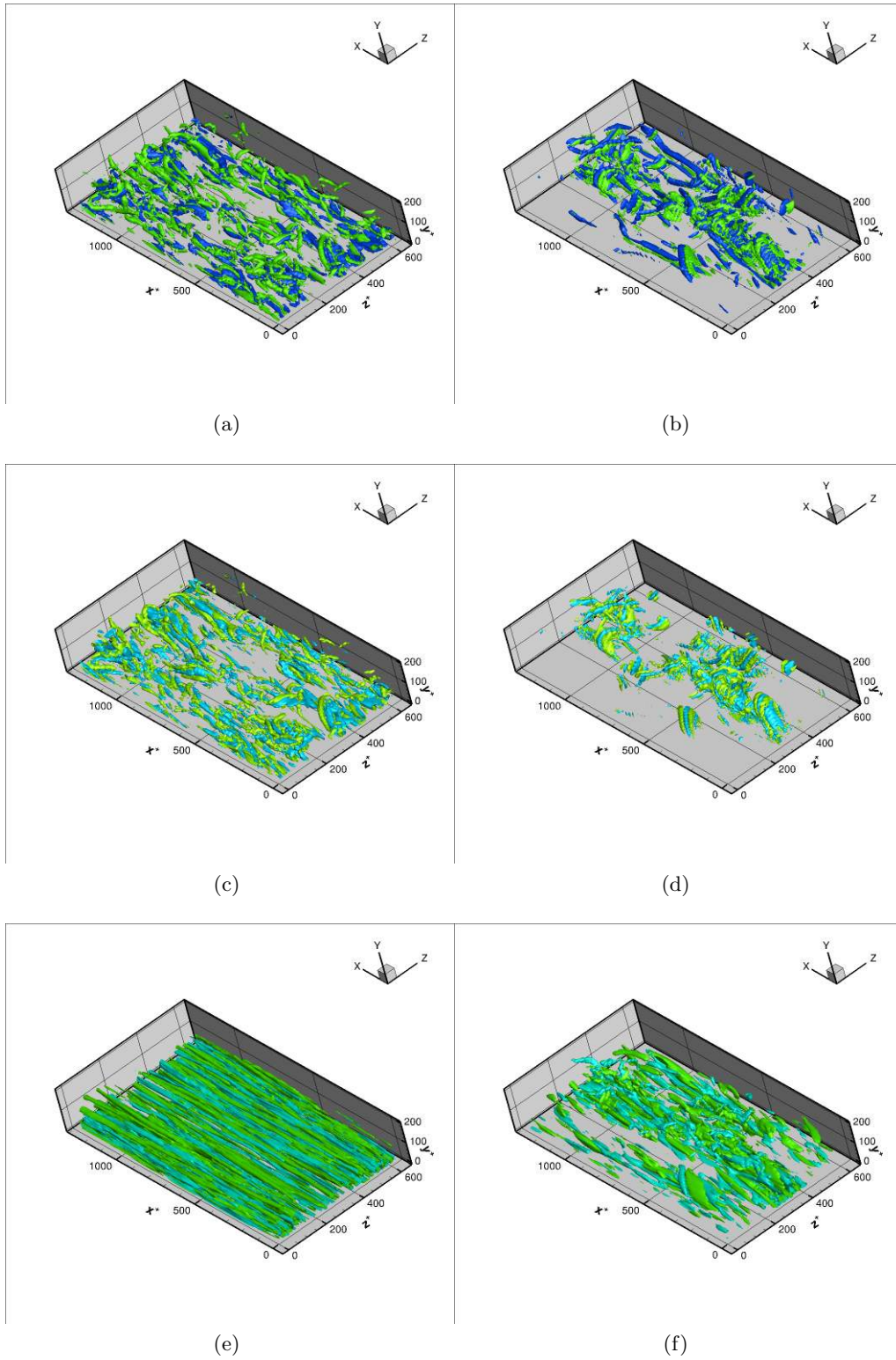
Figure 5: Results for composite analysis on λ_2-C_f snapshots for channel flows: most relevant dynamic modes. reference flow in (a), (c), (e); actuated flowin (b), (d), (f).

References

[1] S. Bagheri. Koopman-mode decomposition of the cylinder wake. *Journal of Fluid Mechanics*, 726:596–623, 7 2013. ISSN 1469-7645. 2

[2] G. Berkooz, P. Holmes, and J.L. Lumley. The proper orthogonal decomposition in the analysis of turbulent flows. *Annual Review of Fluid Mechanics*, 25(1):539–575, 1993. 1

[3] Andrea Cassinelli, Matteo de Giovanetti, and Yongyun Hwang. Streak instability in near-wall turbulence revisited. *Journal of Turbulence*, 18(5):443–464, 2017. doi: 10.1080/14685248.2017.1294757. URL https://doi.org/10.1080/14685248.2017.1294757. 2

[4] K.K. Chen, J.H. Tu, and C.W. Rowley. Variants of dynamic mode decomposition: Boundary condition, Koopman, and Fourier analyses. *Journal of Nonlinear Science*, 22(6):887–915, 2012. 2

[5] D. Duke, J. Soria, and D. Honnery. An error analysis of the dynamic mode decomposition. *Experiments in Fluids*, 52 (2):529–542, 2012. 2

[6] S. Ghebali, J. Garicano-Mena, E. Ferrer, and E. Valero. Identification of flow structures in fully-developed canonical and wavy channels by means of modal decomposition techniques. In *to appear in Journal of Physics: Conference Series, Third Multiflow Summer School on Turbulence.*, 2018. 3, 4

[7] F. Guéniat, L. Mathelin, and L. R. Pastur. A dynamic mode decomposition approach for large and arbitrarily sampled systems. *Phys. Fluids*, 27(2), 2015. doi: 10.1063/1.4908073. 5

[8] M. R. Jovanović, P. J. Schmid, and Joseph W. Nichols. Sparsity-promoting dynamic mode decomposition. *Phys. Fluids*, 26(2), 2014. doi: 10.1063/1.4863670. 3

[9] Paolo Luchini and Maurizio Quadrio. A low-cost parallel implementation of direct numerical simulation of wall turbulence. *J. Comput. Phys.*, 211(2):551–571, January 2006. ISSN 0021-9991. doi: 10.1016/j.jcp.2005.06.003. URL http://dx.doi.org/10.1016/j.jcp.2005.06.003. 1, 3

[10] I. Mezić. Analysis of fluid flows via spectral properties of the Koopman operator. *Annual Review of Fluid Mechanics*, 45(1):357–378, 2013. 2

[11] S. Pope. *Turbulent flows, 2nd Edition*. CUP, 2014. 1, 3

[12] C.W. Rowley, I Mezia, S Bagheri, P Schlatter, and D.S. Henningson. Spectral analysis of nonlinear flows. *Journal of Fluid Mechanics*, 641:115–127, 12 2009. 2

[13] Y. Saad. *Numerical Methods for Large Eigenvalue Problems*. Manchester University Press, Manchester, 1992. 2

[14] Taraneh Sayadi and Peter J. Schmid. Parallel data-driven decomposition algorithm for large-scale datasets: with application to transitional boundary layers. *Theoretical and Computational Fluid Dynamics*, 30(5):415–428, Oct 2016. ISSN 1432-2250. doi: 10.1007/s00162-016-0385-x. URL https://doi.org/10.1007/s00162-016-0385-x. 2

[15] Taraneh Sayadi, Peter J. Schmid, Joseph W. Nichols, and Parviz Moin. Reduced-order representation of near-wall structures in the late transitional boundary layer. *Journal of Fluid Mechanics*, 748:278301, 2014. doi: 10.1017/jfm.2014.184. 2

[16] P.J. Schmid. Dynamic mode decomposition of numerical and experimental data. *J. Fluid Mech.*, 656:5–28, 2010. ISSN 1469-7645. doi: 10.1017/S0022112010001217. 1, 2, 3

[17] C. Viotti, M. Quadrio, and P. Luchini. Streamwise oscillation of spanwise velocity at the wall of a channel for turbulent drag reduction. *Phys. Fluids*, 21(11), 2009. doi: doi.org/10.1063/1.3266945. 1